*Int. J. Electrochem. Sci.*, 12 **(2017)** 7411 – 7425, doi: 10.20964/2017.08.66

**International Journal of**
**ELECTROCHEMICAL**
**SCIENCE**
www.electrochemsci.org

# The Preparation and Electrical Properties of La Doped $Er_{0.2}Ce_{0.8}O_{1.9}$ Based Solid Electrolyte

*Qian Hu*[1], *Fang Yang*[1], *Hao Fang*[1], *Chunhua Zhao*[1,2,*]

[1] Key Laboratory for Ultrafine Materials of Ministry of Education, School of Materials Science and Engineering, East China University of Science and Technology, Shanghai 200237, China
[2] CAS Key Laboratory of Materials for Energy Conversion, Shanghai 200050, PR China
[*]E-mail: zhaochh@ecust.edu.cn

*Received:* 10 May 2017 / *Accepted:* 17 June 2017 / *Published:* 12 July 2017

---

The present trend is to investigate the co-doping approach in ceria either to improve further the electrical conductivity or sintering property. In this study, nano-structured Er and La co-doped ceria powders have been prepared by a novel solid state reaction method. In all the compositions, total dopant cation concentration has been kept at 0.20 atom fraction having general formulae $Ce_{0.8}Er_{0.2-x}La_xO_{1.9}$ ($0 \leq x \leq 0.06$). The phase structure, sintering activity, relative density, microstructure, and electrical properties were characterized by X-ray diffraction (XRD), scanning electron microscope (SEM), and AC impedance spectrum analyzer, respectively. All the samples calcined at 800 ºC crystallized into cubic fluorite structure with the grain size between 20-25 nm, and La content has little impact on the grain size of the powders. SEM shows that the size of the crystal particles is of relatively uniform without pores with La addition 0.02 sintered at 1250 ºC. When the content of La was 0.02, sintered at 1250 ºC measured at 800 ºC, the conductivity reached the maximum value of $3.5\times10^{-2}$ S $cm^{-1}$. Erbium and lanthanum co-doping in $CeO_2$ is a promising electrolyte materials in low-temperature solid oxide fuel cells.

---

**Keywords:** $Ce_{0.8}Er_{0.2-x}La_xO_{1.9}$; La doping; Fluorite structure; Electrical conductivity

## 1. INTRODUCTION

Solid oxide fuel cells which convert chemical energy into electrical energy directly are solid-state devices with a high thermoelectric conversion rates and without pollution [1]. Currently, the ceria-based electrolytes material which could run at the intermediate-low temperature gains widespread concern, and are the most promising electrolyte materials in solid oxide fuel cells [2].

Alkaline-earth or rare-earth elements are commonly used to increase the conductivity of ceria. Researchers have extensively and systematically investigated the electrical properties of ceria-based oxides doped by different elements ($La^{3+}$, $Er^{3+}$, $Sr^{2+}$, $Ca^{2+}$, $Nd^{3+}$, $Sm^{3+}$, $Gd^{3+}$, et al.) with different concentrations [3-11]. Usually, rare-earth doping can get better electrical activity and stability than alkaline-earth doping. The ionic radius of the doped element has a great influence on the electrical properties. If the ionic radius of the doped element has a much difference with that of $Ce^{4+}$, it will cause great lattice expansion and contraction, thereby reducing the electrical conductivities and stability. A little increase in lattice constant is in favor of oxygen ion conduction. Sm and Gd doping lead to a little increase of lattice of ceria and high oxygen ion conductivity can be get. Er doping lead to a little decrease of lattice and the ion conductivity of Er doped samples is lower than Sm and Gd doped samples [12]. Therefore, the ion conductivity of Er doped ceria may be improved by doping an element with a higher ion radius. The ionic radius of $La^{3+}$ (0.116 nm) is much higher than that of $Sm^{3+}$ (r = 0.1130 nm), $Gd^{3+}$ (r = 0.1110 nm), and $Er^{3+}$ (r = 0.1004 nm). Er and La alone doped ceria have been reported, but no reports were given about La and Er co-doping on the electrical properties of ceria [13-16]. Literature is not definite on the issue of effect of La and Er co-doing. In the present investigation $Ce_{0.8}Er_{0.2\text{-}x}La_xO_{1.9}$ has been selected as the base composition. Trivalent dopant $Er(AC)_3 \bullet 4H_2O$) has been substituted by divalent dopant ($La(AC)_2$) keeping the total dopant concentration at 0.20 and the ionic conduction behavior Er and La co-doped ceria has been studied.

Usually, a temperature higher than 1400 ºC is needed for the full densification of ceria based materials. First, such high sintering temperature needs high energy consumption. second, the co-sintering of ceria based electrolyte and electrode for SOFC at high temperature will decrease the porosity of the electrode materials which will decrease the cell output. Therefore, decreasing the densification temperature of ceria based electrolyte becomes very important. This densification temperature can be reduced by improving the sintering activity of ceria based powders. There are two main methods used for preparation of ceria based powders, namely, wet-chemical method and solid state reaction method. The powder prepared by the wet-chemical method has small particle size and high sintering activity. But wet-chemical method includes complicated processing steps and can only produce a small amount of power each time which limits its commercialization. The traditional solid state reaction method has the relatively less processing steps and low cost, but the powder prepared is less active in sintering due to the large particle size caused by the high calcination temperature.

In this paper, a novel solid state reaction method was adapted for the preparation of La doped $Er_{0.2}Ce_{0.8}O_{1.9}$, the effects of La and Er co-doing on the lattice parameters and electrical properties of ceria were studied. In this method, a solid state coordination compound is formed by milling of starting raw materials at temperatures, which is then subjects to calcination at elevated temperatures to yield powders. Relative to wet-chemical method, this method has the advantage of producing a large number of powder at a time. At the same time, nano-scaled particles with high sintering activity can be got by this method.

## 2. EXPERIMENTAL

### *2.1 Fabrication of $Ce_{0.8}Er_{0.2\text{-}x}La_xO_{1.9}$*

The Powders with the nominal compositions $Ce_{0.8}Er_{0.2\text{-}x}La_xO_{1.9}$ ($x$ = 0, 0.02, 0.04, 0.06) were prepared by a novel solid state reaction. Analytical-grade $Ce(AC)_3 \bullet 1.5H_2O$, $Er(AC)_3 \bullet 4H_2O$, $La(AC)_2$, and $H_2C_2O_4 \cdot 2H_2O$ were used as raw materials. A mixture of these acetates and oxalic acid with a molar ratio of total metal ions: oxalic acid of 1 : 1.5 was milled at room temperature for 5 h in a polyethylene container using zirconia balls as the milling medium and ethanol as the dispersion agent until a uniform paste was gained, which indicated the starting materials have thoroughly reacted. Then the precursor was dried and calcined.

In order to improve powders' flowability, the powders calcined at 800 ºC were granulated using Polyvinyl Vinylalcohol Alcohol (PVA) solution. PVA (n = 1750, Shanghai Chemical Reagent Co. Ltd., China) was dissolved in deionized water to get the 5 % solution of PVA. 10 wt % (relative to the calcined powder) PVA solution and the calcined powder were mixed in a mortar, and sieved. Disk-shaped powder compacts of diameter 5 mm and thickness 3 mm were formed by uniaxial pressing at 200 MPa. The powder compacts were heated in air to 400 ºC at a rate of 100 ºC / h and kept at that temperature for 2 h to remove the organic binder, and sintered at 1050 ºC, 1150 ºC, 1250 ºC, and 1350 ºC and kept at that temperature for 5 h for sintering, and then furnace-cooled to room temperature.

### *2.2 Measurements*

Wide-angle (10-80º, 40 kV / 200 mA) powder X-ray diffraction (XRD) was conducted using an X-ray diffraction meter with Cu Ka ($\lambda$ = 0.15406 nm). The range of $2\theta$ = 20-80º was used for all samples in a continuous scan mode with a scanning step size of 0.02º and at a scan rate of 2º / min.

The microstructures of the sintered ceramics were observed with a Hitachi S4800 scanning electron microscope (SEM). The samples were pre-coated with a several nanometers thick layer of gold before observation.

The densification of $Ce_{0.8}Er_{0.18}La_{0.02}O_{1.9}$ was measured by calculating the linear shrinkage. The linear shrinkage is defined as $\Delta L / L_0 = (L_0\text{-}L_T) / L_0$, in which $L_0$ and $L_T$ are the lengths before and after sintering.

For measuring the electrical conductivity, the two opposite sides of the sintered disks were polished and coated with silver paste, heated at 600°C for metallization and furnace-cooled to room temperature. Gold wires were attached as electrode leads. The electrical resistance were measured in the temperature range of 400-800 ºC with 50 ºC interval, using an electrochemical impedance spectrum analyzer (CHI660E, Shanghai Chenhua Inc. China) in the frequency range of 0.1-100 kHz. The resistivity was calculated using the following equation: $\rho = RS / L$, where $R$ is the resistance at different temperatures ($\Omega$), $S$ is the effective area of the pellet ($cm^2$), and $L$ is the thickness of the pellets (cm).

## 3. RESULTS AND DISCUSSION

### *3.1 Formation of mixed Ce-Er-La mixed oxalate*

After milling the acetates and oxalic acid for 5 min, water and acetic acid appeared, indicating the occurrence of reaction. After milling for 5 h, a paste product formed. The paste products were dried at 80 ºC for 10h. The reaction products of 1 # $Er(AC)_3 \cdot 4H_2O$ and $H_2C_2O_4 \cdot 2H_2O$, 2 # $La(AC)_2$ and

$H_2C_2O_4 \cdot 2H_2O$, 3 # $Ce(AC)_3 \cdot 1.5H_2O$ and $H_2C_2O_4 \cdot 2H_2O$, and 4 # the mixture of $Er(AC)_3 \cdot 4H_2O$, $La(AC)_2$, $Ce(AC)_3 \cdot 1.5H_2O$ (Er: La: Ce=0.16 : 0.04 : 0.8) and $H_2C_2O_4 \cdot 2H_2O$ were measured by XRD, as shown in Fig. 1. The product of 3 # is ceria oxalate, which corresponds to the PDF card of JCPDS: 51-0548. The XRD results proved a mixed oxalate formed for 4 # due to the same XRD patterns of 3 # and 4 #, which are distinctly different from that of 1 # and 2 #.

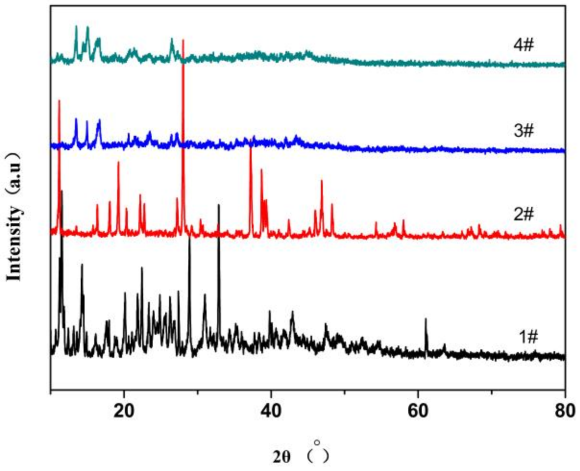

**Figure 1.** The X-ray patterns of the XRD patterns of the reaction products of 1 # $Er(AC)_3 \cdot 4H_2O$ and $H_2C_2O_4 \cdot 2H_2O$, 2 # $La(AC)_2$ and $H_2C_2O_4 \cdot 2H_2O$, 3 # $Ce(AC)_3 \cdot 1.5H_2O$ and $H_2C_2O_4 \cdot 2H_2O$, and 4 # the mixture of $Er(AC)_3 \cdot 4H_2O$, $La(AC)_2$, $Ce(AC)_3 \cdot 1.5H_2O$ (Er : La : Ce = 0.16 : 0.04 : 0.8) and $H_2C_2O_4 \cdot 2H_2O$.

### *3.2 Phase structure, sintering behavior, and microstructure of $Ce_{0.8}Er_{0.2-x}La_xO_{1.9}$*

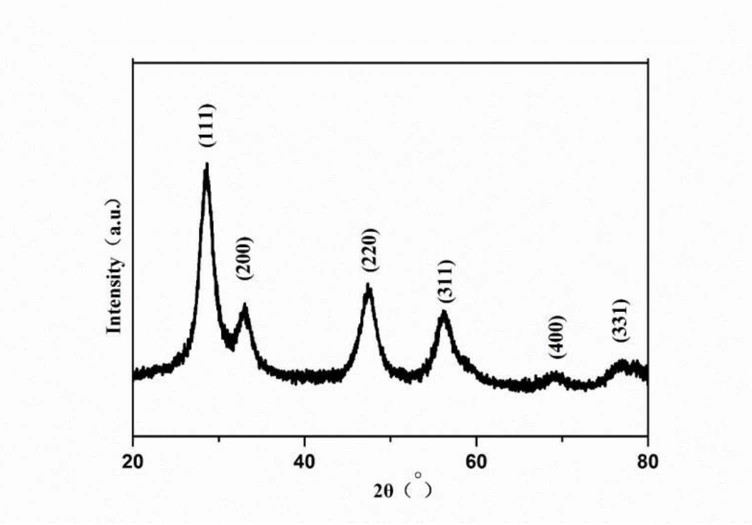

**Figure 2.** The XRD patterns of the reaction products of $Er(AC)_3 \cdot 4H_2O$, $La(AC)_2$, $Ce(AC)_3 \cdot 1.5H_2O$ (Er : La : Ce = 0.16 : 0.04 : 0.8) and $H_2C_2O_4 \cdot 2H_2O$ calcined at 350 ºC.

The product of 4 # was calcined at 350 ºC, and the XRD result was given in Fig. 2. All the peaks are well indexed as a cubic fluorite structure (JCPDS : 34-0394). According to the raw materials used, the product of 4 # is fluorite structured $Ce_{0.8}Er_{0.16}La_{0.04}O_{1.9}$. This XRD result proves that the phase formation temperature here is much lower than that of ceria based electrolyte prepared by other methods. The X-ray diffraction patterns show broad diffraction peaks indicating nano-crystalline nature of powders. The average crystallite size was calculated from X-ray line broadening data using the Scherrer's formulae: $d=K\lambda / \beta\cos\theta$, where, d is the average crystallite size, K is the Scherrer constant, λ is the wavelength of X-ray, 2θ is the Bragg angle, and β is corrected full width at half maximum (FWHM). Scherrer constant K, also called shape factor, varies from 0.89 for spherical to 0.94 for cubic particles. Usually, it is set to 0.9 for particles of unknown size. Here we don't know the exact shape of our powders, so we set is as 0.9. In our work, it is not so important to get the accurate grain size. We just want to prove the powders obtained at 800 ºC has small grain size.

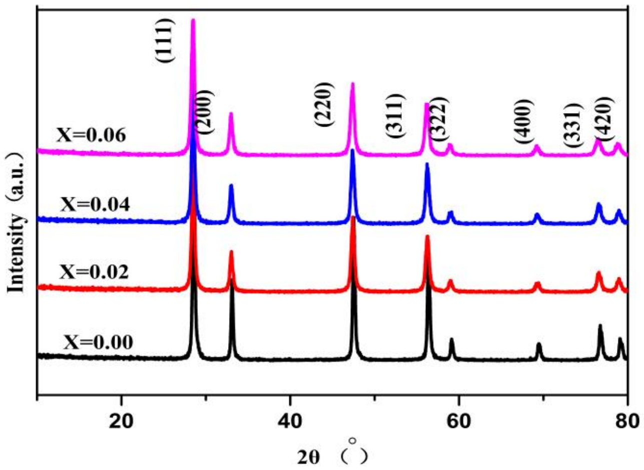

**Figure 3.** The XRD patterns of $Ce_{0.8}Er_{0.2-x}La_xO_{1.9}$ sintered at 800 ºC

The strongest peak corresponding to plane (111) has been considered for the measurement. The grain size of $Ce_{0.8}Er_{0.16}La_{0.04}O_{1.9}$ calcined at 350 ºC is 7 nm. In our work, we found that it was very different to get perfect compacts by dry pressing the powders with the grain size lower than 10 nm. Then we improved the calcining temperature to 800 ºC, and their XRD patterns were given in Fig. 3. All the samples also crystallized into cubic fluorite structure with the grain size between 20-25 nm, and La content has little impact on the grain size of the powders. The grain size of 20-25 nm still has good sintering activity. And perfect green compacts can be obtained by dry pressing.

The lattice constant and lattice volume of $Ce_{0.8}Er_{0.2-x}La_xO_{1.9}$ were measured by using the software of Unit Cell, as shown in Table 1. The lattice constant and volume increase with the increase of La content due to the larger ionic radius of $La^{3+}$ (0.116 nm) than $Er^{3+}$ (0.1004 nm) [17]. The obtained results are in good agreement with the ones presented in the work of Dirstine [18].

**Table 1.** The lattice constants of $Ce_{0.8}Er_{0.2-x}La_xO_{1.9}$ ($x$ = 0, 0.02, 0.04, 0.06)

| $x$ | Lattice constant a(Å) | Lattice volume V(Å)$^3$ |
|---|---|---|
| 0.00 | 5.4025 | 157.6828 |
| 0.02 | 5.4161 | 158.8766 |
| 0.04 | 5.4233 | 159.5111 |
| 0.06 | 5.4368 | 160.7053 |

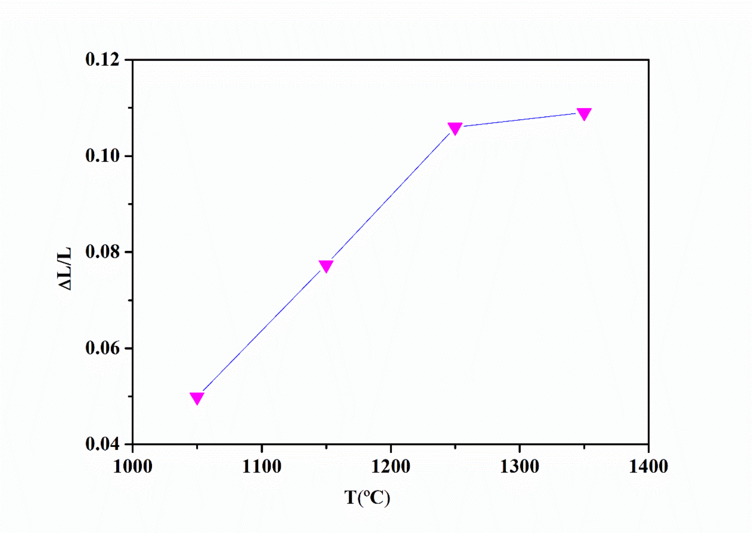

**Figure 4.** The linear shrinkage of $Ce_{0.8}Er_{0.18}La_{0.02}O_{1.9}$ sintered at 1050 ºC, 1150 ºC, 1250 ºC, and 1350 ºC.

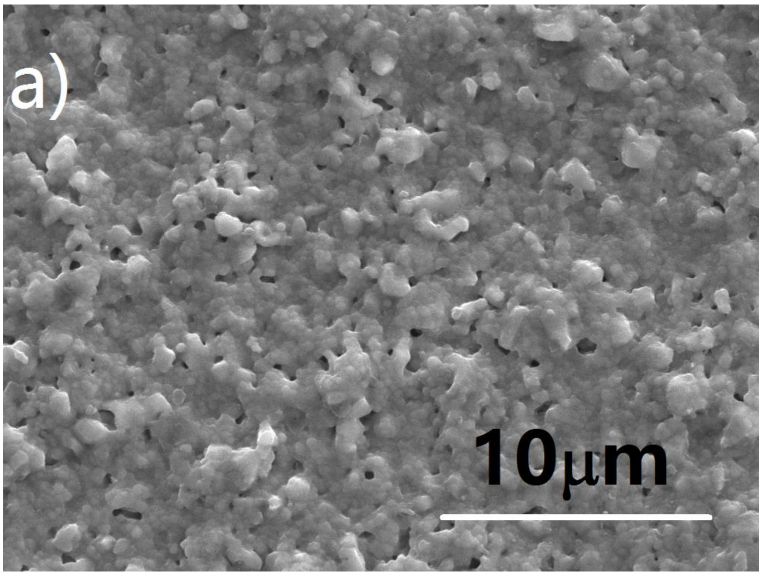

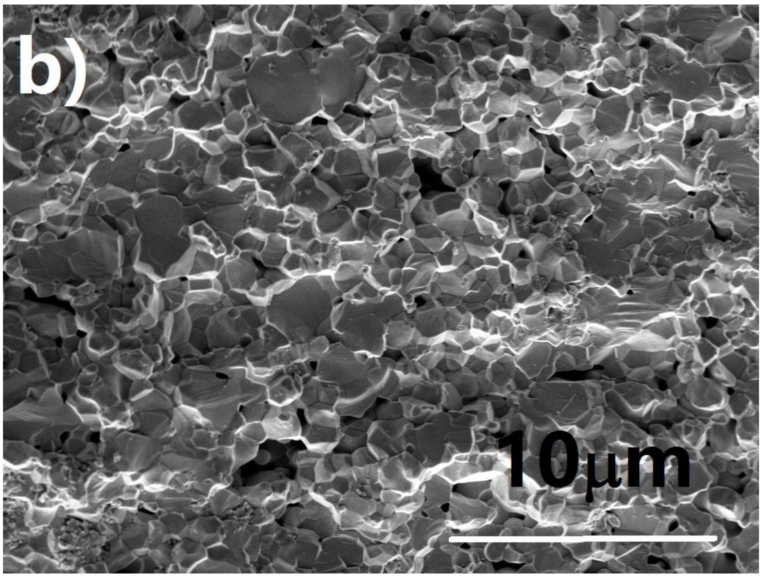

**Figure 5.** The SEM micrographs of $Ce_{0.8}Er_{0.18}La_{0.02}O_{1.9}$ sintered : a) 1250 ºC, and b) 1350 ºC for 5h in air atmosphere.

Fig. 4 gives the linear shrinkage of $Ce_{0.8}Er_{0.18}La_{0.02}O_{1.9}$ sintered at 1050 ºC, 1150 ºC, 1250 ºC, and 1350 ºC. The shrinkage rate of $Ce_{0.8}Er_{0.18}La_{0.02}O_{1.9}$ increases sharply with increase of sintering temperature from 1050 ºC to 1250ºC, and almost no shrinkage is observed from 1250 ºC to 1350 ºC. The densities sintered at 1250 ºC and 1350 ºC are higher than 95% which are dense enough as SOFC electrolyte. The increase in relative density can lead to the increase in conductivity due to the insulation of the pores [19] On the one hand, sintering at 1250 ºC is more energy saving than sintering at 1350 ºC. More energy can be saved at lower sintering temperature. On the other hand, the lower sintering temperature can reduce the reaction between electrolyte and electrode materials of SOFC. Therefore, considering the energy saving and the practical application in SOFC, 1250 ºC is the most suitable sintering temperature.

Fig. 5 gives the microstructure of $Ce_{0.8}Er_{0.18}La_{0.02}O_{1.9}$ sintered at 1250 ºC, and 1350 ºC. The SEM image of the sample sintered at 1250 ºC shows relatively uniform grain size. "uniform" means the grain size is similar and no abnormal grain growth is observed. The rapid densification for the La, Er-doped samples at relative lower sintering temperatures can be attributed to the formation of La, Er-rich liquid phase films in the grain boundaries. The effective liquid phase diffusion under capillary action and the subsequent acceleration of mass transport via a dissolution–precipitation mechanism results in rapid densification and grain coarsening [20]

### *3.3 Electrical properties*

The contributions of grain and grain boundary resistivity to the total resistivity were measured using AC impedance spectroscopy. Fig. 6 gives the results of $Ce_{0.8}Er_{0.18}La_{0.02}O_{1.9}$ sintered from 1050 ºC to 1350 ºC and $Ce_{0.8}Er_{0.2-x}La_xO_{1.9}$ sintered at 1250 ºC measured at 800 ºC. The high frequency intercept (the left intercept of the semicircle) with the real axis represents the grain interior resistivity, the low frequency intercept (the right intercept of the semicircle) corresponds to the total resistivity, and the difference between the high frequency and low frequency intercepts represents the apparent grain boundary resistivity [21].

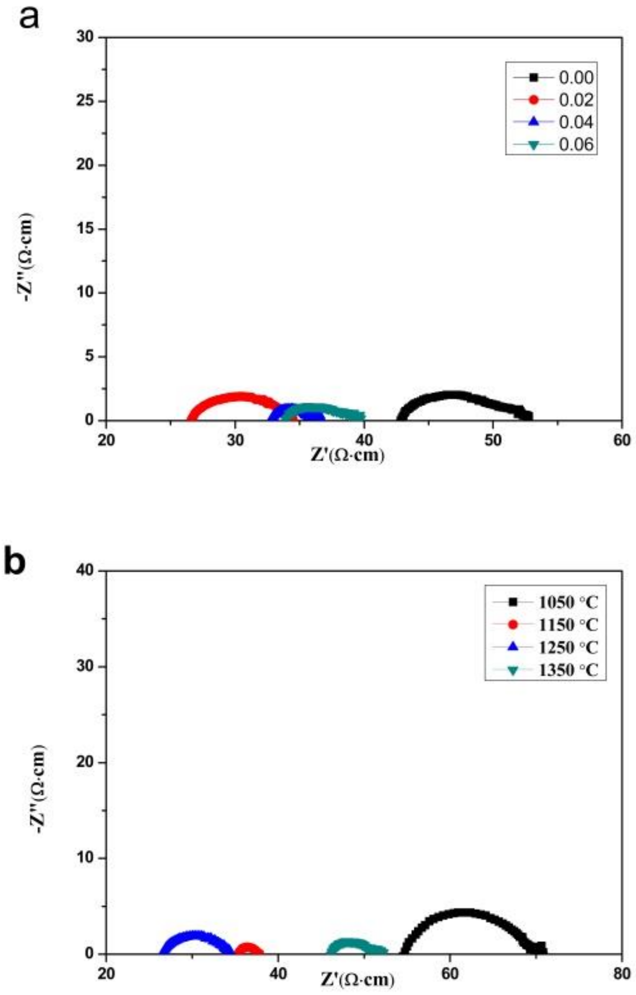

**Figure 6.** The AC impedance spectroscopy measured at 800 ºC: a) Ce0.8Er0.2-xLaxO1.9 sintered at 1250ºC , b) Ce0.8Er0.18La0.02O1.9 sintered from 1050 ºC to 1350 ºC.

The electrochemical impedance of all the samples were measured in the temperature range of 400-800 ºC with 50 ºC interval. One semicircle is observed for all the impedance plots. The grain, apparent grain boundary, and total resistivity can be extracted from the AC impedance spectra. And the conductivities can be calculated according to this equation: $\sigma = 1 / \rho$, where $\rho$ is the resistivity. For the Ce-based electrolyte, the contribution of the electronic conductivity is negligible in air, and therefore conduction comes from the migration of oxygen ions through the oxygen vacancies that provide the migration channels [22]

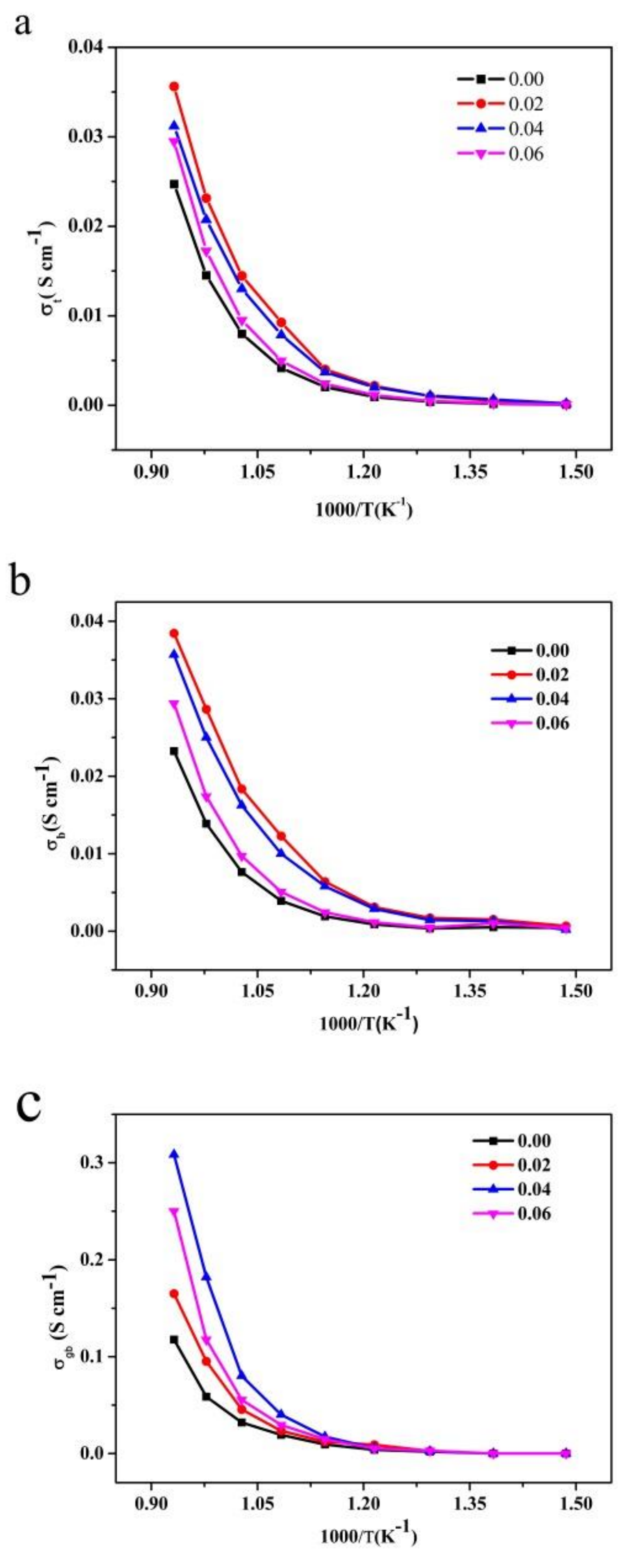

**Figure 7.** The conductivity of $Ce_{0.8}Er_{0.2-x}La_xO_{1.9}$ sintered at 1250 ºC: a) the total, b) the grain, and c) the grain boundary.

Fig. 7 gives that conductivities of $Ce_{0.8}Er_{0.2-x}La_xO_{1.9}$ sintered at 1250 ºC measured from 400 to 800 ºC. The total, grain, and grain boundary conductivities first increase then decrease with increase of La content. When the content of La was 0.02, it reached the maximum value, and the conductivity could reach $3.5\times10^{-2}$ S cm$^{-1}$ at 800 ºC, which is 20% higher than the results obtained in [23-25]. However, it must be emphasized that the novel solid state reaction method is much cheaper than other methods of synthesis[25].The conductivity of $Ce_{0.8}Sm_{0.2}O_{1.9}$ prepared by the same method was also reported. The conductivities of $Ce_{0.8}Sm_{0.2}O_{1.9}$ sintered at 1200 ºC and 1300 ºC measured at 800 ºC are $2.1\times10^{-2}$ S cm$^{-1}$ and $2.9\times10^{-2}$ S cm$^{-1}$, respectively[26]. Here, the conductivity of $Ce_{0.8}Er_{0.18}La_{0.02}O_{1.9}$ is higher than that of $Ce_{0.8}Sm_{0.2}O_{1.9}$. The oxygen vacancy distribution and lattice change affect the grain conductivity. La doping does not result in the change of oxygen vacancy concentration because both of La and Er are trivalent elements. However, double doping (La and Er co-doping) usually can increase the oxygen vacancy disorder which helps to improve the grain conductivity. The increase of lattice constant caused by La doping enlarge the channel of oxygen ion transport which also improves the grain conductivity. Lattice distortion may occur with further increase in La content due to the big difference between the ionic radii of La$^{3+}$ (0.116 nm) than Ce$^{4+}$(0.970Å) [17].

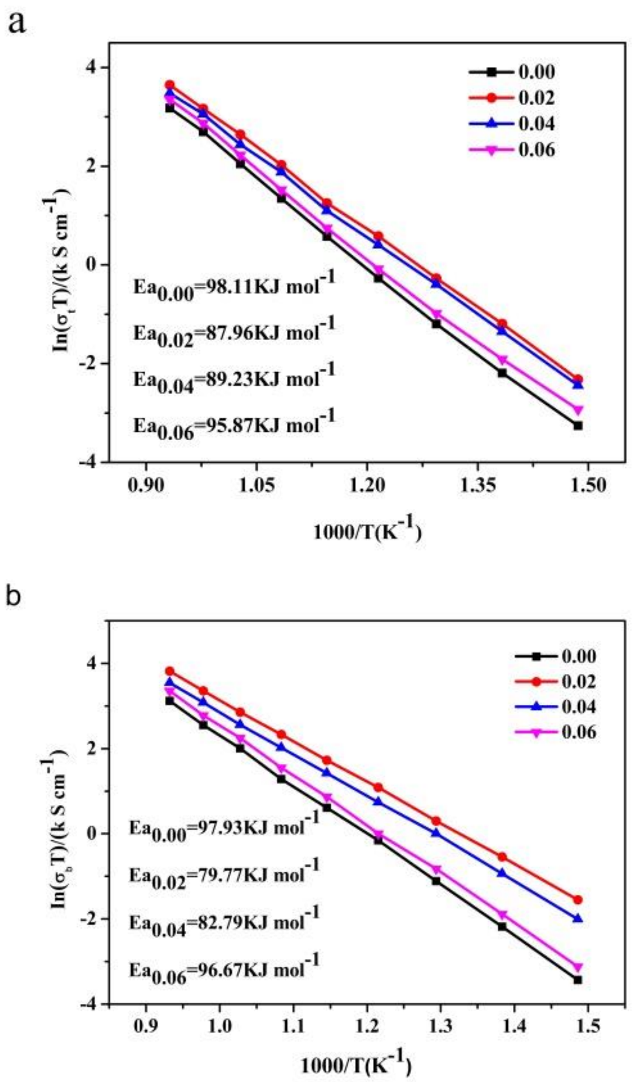

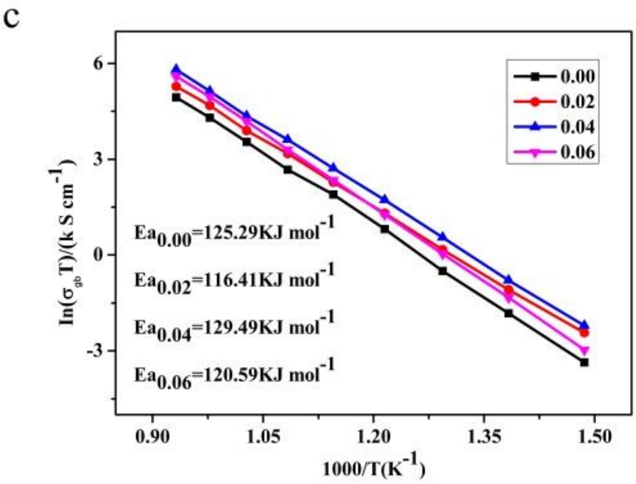

**Figure 8.** The Arrhenius plots of ln(σT) versus 1000 / T for $Ce_{0.8}Er_{0.2-x}La_xO_{1.9}$ sintered at 1250 ºC: a) the total, b) the grain, and c) the grain boundary.

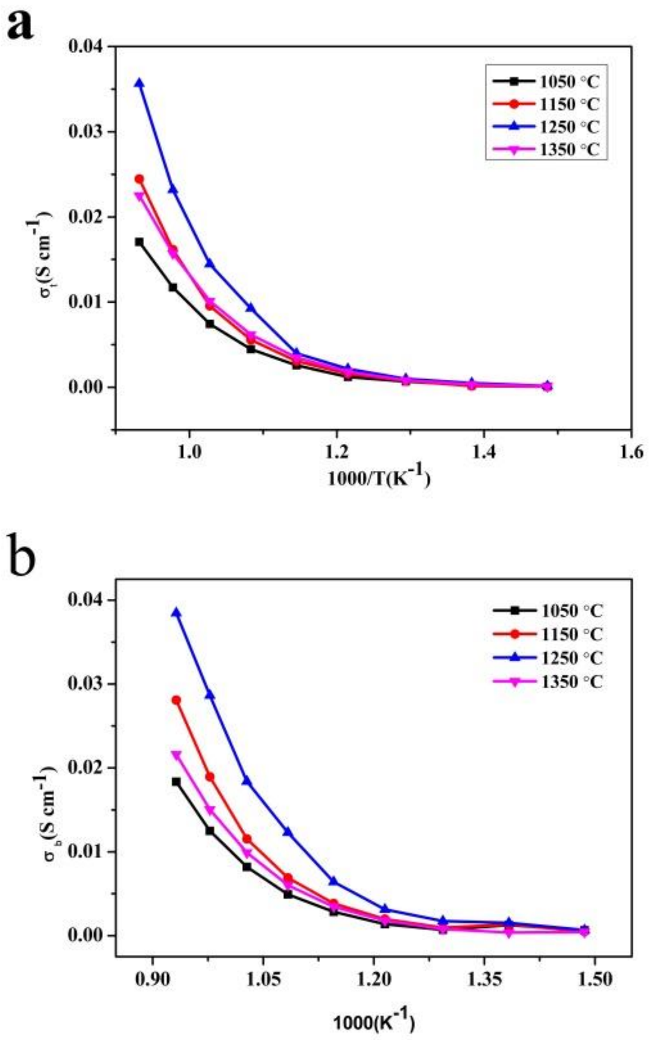

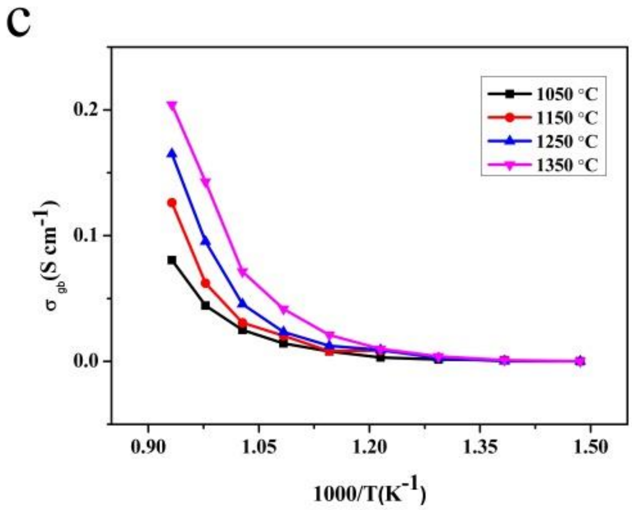

**Figure 9.** The conductivity of $Ce_{0.8}Er_{0.18}La_{0.02}O_{1.9}$ sintered at 1050 ºC, 1150 ºC, 1250 ºC, and 1350 ºC: a) the total, b) the grain, and c) the grain boundary.

The lattice distortion usually leads to the decrease of grain conductivity. With the change of oxygen vacancies and lattice, the grain conductivity increases first and then decreases with the increase of La content. Different grain boundary segregation at La content leads to different grain boundary resistivity. The new formed vacancies and defects could accelerate the mass transport process and increase the sintering rate [27, 28] Fig. 8 give the Arrhenius plots of ln(σT) versus 1000 / T for $Ce_{0.8}Er_{0.2-x}La_xO_{1.9}$. The activation energy of $Ce_{0.8}Er_{0.18}La_{0.02}O_{1.9}$ has the lowest value 87.96 KJ $mol^{-1}$. So, the La optimum doping amount was 0.02.

Fig. 9 indicates that the total, grain, and grain boundary conductivities of $Ce_{0.8}Er_{0.18}La_{0.02}O_{1.9}$ sintered at 1050 ºC, 1150 ºC, 1250 ºC, and 1350 ºC respectively. The grain has comparable conductivity as grain boundary when the measurement temperature is between 400 ºC to 500 ºC, and the total conductivity is determined by both of grain and grain boundary. With the increase of measurement temperature, the grain boundary conductivity increases more quickly than grain conductivity.

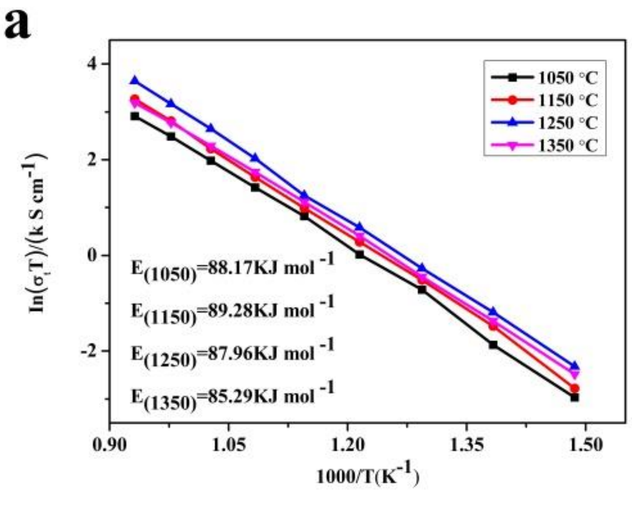

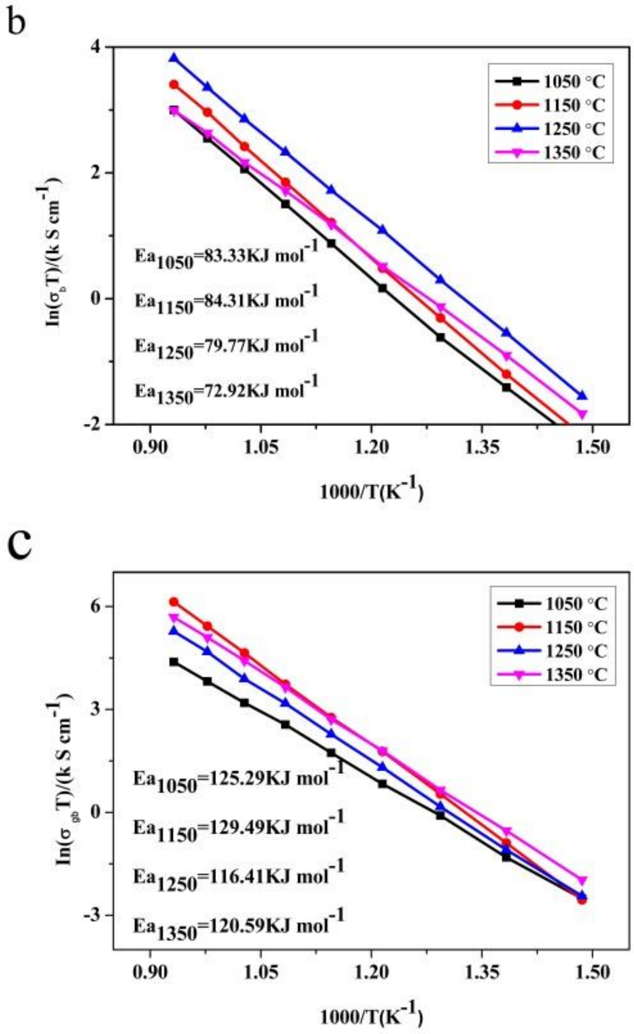

**Figure 10.** The Arrhenius plots of ln(σT) versus 1000 / T for $Ce_{0.8}Er_{0.18}La_{0.02}O_{1.9}$ sintered at 1050 ºC,1150 ºC,1250 ºC,1350 ºC respectively: a) the total, b) the grain, and c) the grain boundary.

The total conductivity is determined by grain conductivity when the measurement temperature is higher than 600 ºC. The total, grain, and grain boundary conductivities obey the Arrhenius relation, Activation energies (Ea) were calculated from the Arrhenius plots ,as shown in Fig. 10.

The grain boundary has much higher activation energy than grain. The total, grain, and grain boundary conductivities first increase then decrease with increase of sintering temperature. Both of the densification and grain size affect the grain conductivity. For the ceramics with poor densification, the pores at the grain or grain boundary weaken the conductive channel, and the migration of oxygen ions is blocked by the pores. The increase of density can led to the obvious increase of grain conductivity. But with the increase of sintering temperature, the grain size also increases which may lead to the decrease of grain conductivity. Different grain boundary segregation at different sintering temperatures leads to different grain boundary resistivity. Based on the published studies of different authors, it can be concluded that the present value of Ea presented in our work is lower compared to the activation energy for single -, co- and multi -doped $CeO_2$(containing 20% of dopants) [29-31].

## 4. CONCLUSIONS

$Ce_{0.8}Er_{0.2-x}La_xO_{1.9}$ ($0 \le x \le 0.06$) oxides was prepared easily by an novel solid state reaction method, which synthesized nanopowders that are single phase and exhibit the fluorite crystal structure. At 1250 ºC, the shrinkage rate reached the maximum at above 0.1, and the corresponding density was more than 95 %, the optimum sintering temperature of the sample is 1250 ºC. The doped lanthanum has a big influence on the conductivity. Compared with other components under the same conditions, $Ce_{0.8}Er_{0.18}La_{0.02}O_{1.9}$ has a stable phase structure, lower activation energy, higher conductivity. The highest values of conductivity in air could reach $3.5\times10^{-2}$ S $cm^{-1}$ in 800 ºC. Therefore, $Ce_{0.8}Er_{0.18}La_{0.02}O_{1.9}$ is a promising electrolyte material.

ACKNOWLEDGEMENTS
This work is supported by National Natural Science Foundation of China (Grant no. 51102094), Opening Project of CAS Key Laboratory of Materials for Energy Conversion, Research Fund for the Doctoral Program of Higher Education of China (Grant no. 20110074120013), Shanghai Leading Academic Discipline Project (Grant no. B502), Shanghai Key Laboratory Project (Grant no. 08DZ2230500).

## References

1. F. Alcaide, P. L. Cabot, E. Brillas, *J. Power Sources*., 153 (2006) 47.
2. T. Mori, J. Drennan, J. H. Lee, J. G. Li, T. Ikegami, *J. Solid State Ion*., 154 (2002) 461.
3. V.V. Kharton, F. M. Figueiredo, L. Navarro, E. N. Naumovich, A.V .Kovalevsky, A. A. Yaremchenko, J. R. Frade, *J. Mate Sci*., 36 (2001) 1105.
4. W. Liu, B. Li, H. Liu, W. Pan, *J. Electrochim Acta*., 56 (2011) 3334.
5. D. Perez-Coll, P. Nunez, J. R. Frade, *J. Power Sources*., 196 (2011) 8383.
6. J. M. S. Júnior, L. F. B. Malta, F. M. Garrison, T. Ogasawara, M. E. Medeiros, *J. Materials Chem. Phys.*, 135 (2012) 957.
7. E. Y. Pikalova, A. A. Murashkina, V. I. Maragou, A. K. Demin, V. N. Strekalovsky, P. E. Tsiakaras, *J. hydrogen energy*., 36 (2011) 6175.
8. H. Bae, J. Choi, G .M. Choi, *J. Solid State Ion*., 236 (2013) 16.
9. J. Wright, A .V. Varchars, *J. Power Sources*., 196 (2011) 6118.
10. J. Jiang, W. Shen, J. L. Hertz, *J. Solid State Ionics*., 249 (2013) 139.
11. M. Kahlaoui, S. Chefi, A. Inoubli, A. Madani, C. Chefi, *J. Ceram Int*., 39 (2013) 3873.
12. T. Mori, H. Yamamura. *J Mater Synth Process*. 79 (1998) 3309.
13. C. Peng, Y. Wang, K. Jiang, B. Q. Bin, H. W. Liang, J. Feng, J. Meng, *J. Alloys Compd*., 349 (2003) 273.
14. A. Sin, Y. Dubitsky, A. Zaopo, A. S. Arico, L. Gullo, D. La Rosa, Ballabio, *J. Solid State Ion*., 175 (2004) 361.
15. M. Stojmenović, S. Bošković, M. Žunić, B. Babić, B. Matović, D. Bajuk-Bogdanović, S. Mentus, *J. Materials Chem. Phys*., 153 (2005) 422.
16. E. Yu, A. A. Pikalova, V. I. Murashkina, A. K. Maragou, Demin, V. N. Strekalovsky, P. E. Tsiakaras, *J. Hydrogen Energy*., 36 (2011) 6175.
17. S. M. Haile, *J. Acta Mater*., 51 (2003) 5981.
18. R. T. Dirstine, R. N. Blumental, T. F. Kuech, *J. Electrochem Soc*., 126 (1979) 264.
19. H. Yoshida, T. Inagaki, *J. Alloys. Compd*., 408 (2006) 632.

20. C. Tseng, P. Chen, P. Lin, *J. Alloys Compd*., 632 ( 2015) 810.
21. S. H. Jensen, A. Hauch, P. V. Hendriksen, M. Mogensen, N. Bonanos, T. Jacobsen, *J. Electrochem. Soc.*, 154 (2007) 551.
22. A. Tsoga, A. Naoumidis, D. Stöver, *Solid State Ionics*., 135 (2000) 403
23. S. Omar, E. D. Wachsman, J. C. Nino, *J. Solid State Ion*., 178 (2008) 1890.
24. X. Guan, H. Zhou, Y. Wang, J. J. Zhang, *J Alloys Comp*., 464 (2008) 310.
25. N. Jaiswal, D. Kumar, S. Upadhyay, O. Parkash, *J. Alloy. Compd.*, 577 (2013) 456
26. Y. Tao, H. Qian, Y. Yang, Z. Chh, *J. Electrochem. Sci*., 11 (2016) 5724.
27. M. Valant, D. Suvorov, R. C. Pullar, K. Sarma, N. M. Alford, *J. Eur. Ceram. Soc*., 26 (2006) 2777.
28. J. Hong, S. Ida, T. Ishihara, *Solid State Ionics*., 262 (2014) 374.
29. W. Liu, B. Li, H. Liu, W. Pan, *J. Electrochim. Acta*., 56 (2011) 3334.
30. D. Perez-Coll, P. Nú~ nez, J.R. Frade, *J. Power Sources*., 196 (2011) 8383
31. N. Jaiswal, D. Kumar, S. Upadhyay, O. Parkash, *J. Alloy. Compd*. ,577 (2013) 456.